Research Square

Preprints are preliminary reports that have not undergone peer review.
They should not be considered conclusive, used to inform clinical practice,
or referenced by the media as validated information.

Cetyltrimethylammonium bromide-metal complex assisted Gold@sulfamerazine nanoconjugates: Synthesis and characterization

Zoya Zaheer

zoya.zaheer@mail.com

King Abdulaziz University

Huda Razayq Alyoubi

King Abdulaziz University

Wafa A. Bawazir

King Abdulaziz University

Research Article

Keywords: Surfactant-metal complex, CTA-AuNPs/SMZ, Sulfamerazine, Morphology

Posted Date: November 19th, 2026

DOI: https://doi.org/10.21203/rs.3.rs-11019941/v1

License: This work is licensed under a Creative Commons Attribution 4.0 International License.
Read Full License

Additional Declarations: No competing interests reported.

Cetyltrimethylammonium bromide-metal complex assisted Gold@sulfamerazine nanoconjugates: Synthesis and characterization

Zoya Zaheer*, Huda Razayq Alyoubi, Wafa A. Bawazir

Department of Chemistry, Faculty of Science, King Abdulaziz University, P. O. Box 80203, Jeddah, 21589, Saudi Arabia

---

Abstract

Cetyltrimethylammonium bromide (CTAB) is one of the most potentially cationic surface-active agents, widely used in DNA extraction, as a strong capping agent in the synthesis of nanomaterials, and in cosmetics. In this work, the formation of cetyltrimethylammonium-$AuCl_4$ complex (CTA-$AuCl_4$, yellow- orange color) was visually observed and characterized by UV-visible spectroscopy and transmission electron microscopy (TEM). The solution color from yellow to bark brown with increasing CTAB concentration resulted from the interactions of $HAuCl_4$ with aggregates of the CTAB with fine anti-interference. The gold@ sulfamerazine nanoconjugates were prepared by the chemical reduction of CTA-$AuCl_4$ in the presence of sodium borohydride. The surface morphology, crystalline nature, position of surface plasmon resonance band (SPR), size distribution, elemental composition, and elemental mapping were established by scanning electron microscopy (SEM), X-ray diffraction (XRD), UV-visible spectroscopy, TEM, and electron dispersive microscopy (EDX), respectively. The ^{1}H and ^{13}C NMR spectroscopy was used to determine the presence of sulfamerazine (SMZ) and CTA^{+} onto the surface of the as-prepared AuNPs. XRD patterns reveal the formation of face-centered cubic metallic gold with space group = 225: $Fm\bar{3}m$: lattice constant ($\alpha = \beta = \gamma = 90.00^{0}$, a = b = c = 0.4076 nm, and V = 67.745 $Å^3$), crystallite size = 2.283 nm, strain = 0.00 %, and content = 100 %. Surfactant metal complex, CTA-

$AuCl_4$ can itself act as a source of metal ions and nanoparticle protectors for the fabrication of advanced nanomaterials with desired morphology for industrial and medicinal applications.

Keywords: Surfactant-metal complex; CTA-AuNPs/SMZ; Sulfamerazine; Morphology

---

***Corresponding Author: Zoya Zaheer (zoya.zaheer@mail.com (Z. Zaheer)**

1. Introduction

Several methods have been used to determine the behaviors of cationic surfactants. Some investigators describe the utilization of the ion-pair extraction and UV-visible spectroscopy for the aggregation of cationic surfactants with organic dyes [1, 2]. Buwalda et al. [3] reported the shifts of absorption maxima in an aqueous solution of methyl orange and various dicationic surfactants at a constant concentration of the methyl orange with different concentrations of the cationic surfactants. Dikaky et al. utilized the UV-visible spectroscopy to determine the ionization constant and thermodynamic parameters of acid alizarine violet in micellar solutions of CTAB, TX-100, and SDS [4]. Generally, cationic surfactants, especially CTAB, were used for the removal of dyes from an aqueous solution [5-7] and as a strong stabilizing agent for the synthesis of plasmonic nanomaterials of gold [8-11], silver [12] and copper [13] to stabilize the shape, which forms an ordered layer on the surface of the nanoparticles.

The AuNPs show potential biological as well as chemical applications in biosensing, drug delivery, and photothermal therapeutics due to their tunable plasmonic properties [14, 15], anisotropic shape, and ease of functionalization [16]. The AuNPs have been prepared by using the different methods, such as chemical reduction [17-19], green synthesis [20], coprecipitation [21], sol-gel [22], microwave-assisted [23], laser ablation [24], microemulsion [25], and others [26] for various applications. The AuNPs can be categorized into various types-based morphology (size, shape, and the size distribution), which depends on the method of preparation employed [27]. The size and uniformity are controlled by the reaction conditions and the nature of the stabilizing agent used [28]. Sagle et al. developed a simple one-pot

method for the complete removal of CTAB from the surface of gold nanorods by using sodium borohydride and mercaptoundecanoic acid for better biological in vivo studies [29]. Li et al. prepared citrate stabilized AuNPs by the chemical reduction method, modified by the addition of sulfadiazine, and used them as a sensor for the rapid colorimetric detection of Hg^{2+} ions [30].

Sulfonamides (sulfa drugs) are the synthetic most used broad-spectrum antibiotics due to their low cost and high efficiency towards bacterial and protozoal infections. Niu et al. [31] used para-sulfonatocalix[4]arene stabilized AuNPs for the colorimetric detection of sulfamethazine via host-guest interaction. The AuNPs can be used as a nanozyme (nanomaterial with enzyme-like properties) because these NPs show outstanding catalytic activity towards the reduction of hydrogen peroxide [32]. Yang et al. [33] developed an electrochemical biosensor (Ag^{+}@ CTAB-AuNPs complex) and used it for the rapid detection of sulfamethazine in aquatic environments. Zhang and his coworkers reported that the Ag(I) ions competitively combined with CTAB on the surface of CTAB-AuNPs and enhanced the catalytic activity of the nanomaterials significantly [34].

Xiao and Qi [35] reported the role of surfactants in the shape-controlled synthesis of AuNPs by using general strategies, such as single surfactants, mixed surfactants, supramolecular surfactants, and metal-surfactant complex templates. Qi et al. [36] prepared metal-surfactant complex template precursor nanobelts by using $HAuCl_4$ and $Br^{-}[(CH_3)_3N^{+}\text{-}(CH_2)_{12}\text{-}N^{+}\text{-}(CH_3)_3]Br^{-}$ (bolaform surfactant containing two quaternary ammonium head groups), and the as-prepared complex was reduced to the gold nanocrystals with $NaBH_4$. Kaur and Mehta [37] and Jia and Schuth [38] reviewed the role of self-aggregating metal-surfactant complexes (metallosurfactants) acts as nanoreactors for the precursor of nanoparticle formation and

thermal decomposition of metal surfactant complexes, respectively. However, to the best of our knowledge, the synthesis of gold nanoparticles by using a gold-surfactant complex (metallosurfactant) template is still rather limited except for the studies investigating the reduction of a surfactant-gold salt complex into nanobelts in the presence of $NaBH_4$.

This study aims to prepare AuNPs using CTA-$AuCl_4$ self-aggregating complex and functionalized with SMZ. This method involves first adding of $HAuCl_4$ in the solution of CTAB. Immediately, the solutions of SMZ and $NaBH_4$ are added to the same solution. Lastly, the decay of resulting orange-color absorbance by $NaBH_4$ was monitored at different time intervals using UV-visible spectroscopy. Therefore, this study describes a UV-visible spectrophotometric technique to identify the formation of a surfactant metal complex (CTA-$AuCl_4$, a metallosurfactant) in an aqueous solution. Upon the addition of $HAuCl_4$, the CTA^+ (ionized species of CTAB, $CTAB \rightarrow CTA^+ + Br^-$) interacts via electrostatic response and therefore results in complexation with the CTA^+ accompanied by a shift to a higher wavelength. The complexation provides a color modulation, which allows the detection of CTAB by the naked eye; the plasmonic peak in the visible region allows quantification of CTAB in the absence of a strong reducing agent for the first time. CTA-$AuCl_4$ was reduced with $NaBH_4$ in the presence of SMZ, and resulting gold sols exhibit a sharp SPR peak at 537 nm. The ^1H NMR and ^{13}C NMR spectroscope was used to identify the presence of the CTAB and SMZ on the surface of the AuNPs.

2.Experimental section

2.1. Materials

Gold(III) chloride trihydrate ($HAuCl_4.3H_2O$, molar mass = 393.83 g/mol, purity = ≥ 99.9%), sulfamerazine ($C_{11}H_{12}N_4O_2S$, molar mass = 264.30 g/mol, purity = ≥ 99.0%), cetyltrimethylammonium bromide ($C_{16}H_{42}BrN$, molar mass = 364.45 g/mol, purity = ≥ 98.0%), sodium borohydride ($NaBH_4$, molar mass = 37.83 g/mol, purity = ≥ 98.0%) were received from Sigma-Aldrich. All reagents were used without further purification. Double-distilled and CO_2 free water was used as solvent for the preparation of all aqueous solutions.

2.2. Instrumentation

UV-visible absorption spectra were recorded on a Varian Cary 500 spectrophotometer using 1 cm path length quartz cuvettes at a wavelength range from 200 to 800 nm. The FTIR spectra were executed on a Perkin-Elmer 293 spectrophotometer at a wavelength range 500-4000 cm^{-1}**.** Nuclear-magnetic-resonance (^1H NMR and ^{13}C NMR) spectra were executed on a Bruker Advance III spectrometer at 500 MHz in dimethyl sulfoxide solution. Tetramethyl silane was used for the determination of chemical shifts. Transmission electron microscope (TEM), scanning electron microscope (SEM), and electron-dispersive X-ray spectroscopy (EDX) were utilized for the evaluation of the size, shape, distribution, surface morphology, elemental composition, and elemental mapping of the SMZ-modified CTA@AuNPs. TEM samples were prepared by placing a drop of the aqueous suspension on a copper gride with a continuous carbon film coating, followed to dry naturally (solvent evaporation) at room temperature. X-ray diffraction (XRD) patterns were recorded using the Bruker advanced spectrometer with a 2θ range of 5.0^0 to 90^0, a step size of 0.02^0, a scan speed/duration time of 4.00 degrees/min, a current of 40 mA, a voltage of 40 kV, and a Cu Kα (λ = 1.54060 Å). All analyses were performed at room temperature (23 ^0C).

2.3. Preparation of CTA@AuNPs/SMZ

For the preparation of the CTA-$AuCl_4$ ion-pair, 5mL of $HAuCl_4$ solution in 50 mL of deionized water and 2.0 mL of CTAB (0.01 mol/L) solution were mixed under stirring in a constant-temperature water bath. The color of the solution changes from the pale yellow of the original $HAuCl_4$. $3H_2O$ to a distinct orange immediately [39]. The UV-visible spectra of $HAuCl_4$, CTAB, and the reaction mixture (CTAB + $HAuCl_4$) were recorded at different time intervals. After that, the solution was transferred in to a glass bottle and stored in a dark place at room temperature for several weeks. The SMZ (5.0 mL of 0.01 mol/L) and 2.0 mL of $NaBH_4$ (0.01 mol/L) solutions were added into the reaction mixture. The orange color changes to brown-purple after the addition of $NaBH_4$ slowly. To determine the SPR band of resulting AuNPs, the progress of the reaction was followed by recording the UV-visible spectra of the resulting sols as a function of time. The as-prepared AuNPs are centrifuged at 5000 rpm for 10 min, filtered, washed with deionized water, then bottled, and stored in a refrigerator at 5 ^{0}C for subsequent use.

3.Results and discussion

3.1. Formation of CTA-$AuCl_4$ nanoconjugates

Visual observations indicate that the colorless aqueous solution of CTAB became orange after the addition of a $HAuCl_4$ solution at room temperature immediately. The interactions between the CTAB and $HAuCl_4$ were examined through UV-visible spectroscopy. Fig. 1 illustrates the UV-visible spectrum of the $HAuCl_4$ aqueous solution alongside the spectra of the resulting orange color at definite time intervals at two different concentrations of the CTAB (1.0 and 2.0 mM, respectively, for Fig. 1A and Fig. 1B) at a constant $HAuCl_4$ concentration (0.6 mM). The $HAuCl_4$ solution exhibits two pronounced absorption peaks at 232 nm (strong peak) and 296 nm (weaker peak) in the ultra violet region due to the ligand to metal charge transfer. The former

peak is the characteristic of Au(III) complexes and is often used to monitor the presence of Au(III) precursor during AuNPs preparation [26, 40]. Interestingly, the shape of the $HAuCl_4$ spectrum changed markedly after the addition of CTAB, and an orange color appeared with the mixing time, which exhibits four absorption peaks at 248 nm, 303 nm, 409 nm, and 464 nm. The difference in the spectrum of $HAuCl_4$ (Fig. 1) from the resulting orange color could be detected by the appearance of absorption peaks at the longer wavelength of 248 and 303 nm in the ultra violet region, likely indicating the formation of an ion-pair between the CTAB and gold salt precursor.

The optical properties of $HAuCl_4$ -CTAB reaction mixture strongly depends on the concentrations of the $HAuCl_4$ as well as the CTAB concentrations. Figs. S1 and S2 (supporting information) show the effect of $HAuCl_4$ and CTAB concentrations on the peak intensity and the positions of the absorption peaks. As shown in Fig.1, S1, and S2, when $HAuCl_4$ interacted with CTAB, the maximum absorption peaks appear in the visible region from 400 to 470 nm. Notably, the appearance of a yellow-orange color as well as the prominent absorption peak centered at 409 nm and a broad shoulder band at 464 nm favorably supports the formation of gold(III)-CTAB nanoconjugates with anisotropic morphology.

Fig. 2A shows that the absorbance of absorption peak at 403 nm increases with increasing the CTAB concentrations, until it reaches to a maximum, and then became constant. The above observations indicate that the addition of the $HAuCl_4$ in to the CTAB solution resulted in the appearance of an orange color, which could be ascribed to the formation of CTA-$AuCl_4$ (Eq. 1).

$$CTAB + HAuCl_4 = CTA - AuCl_4 + HBr \qquad (1)$$

Eq. (2) was used to determine the CTA-$AuCl_4$ formation constant (K_S) [41, 42] with slight modification.

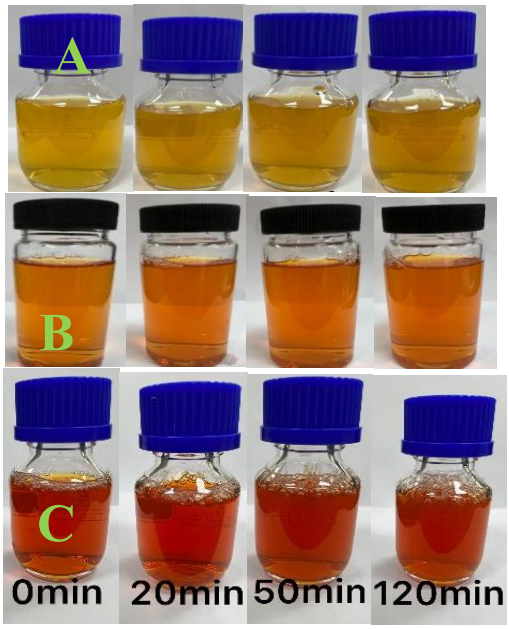
$$\frac{[CTAB][HAuCl_4]}{A} = \frac{[CTAB]}{\varepsilon . l} + \frac{1}{K_S \varepsilon . l} \qquad (2)$$

where A is the difference in absorbance between the CTA-$AuCl_4$ ion-pair and CTAB at the wavelength (400 nm) where both complexed and uncomplexed forms of CTAB absorb, ε is the molar absorption coefficient, K_S is the ion-pair formation constant, and l is the path length (1 cm). From Eq. (2), the plot of left-hand side versus [CTAB] should be linear with slope (= 1/ ε) and intercept (= 1/K_S ε) at a constant path length. The ε = 2631.58 mol^{-1} dm^3 cm^{-1} and K_S = 1835.55 mol^{-1} dm^3, respectively, were calculated from the slope and intercept of the Fig. 2B (y axis = [CTAB] [$HAuCl_4$] / A).

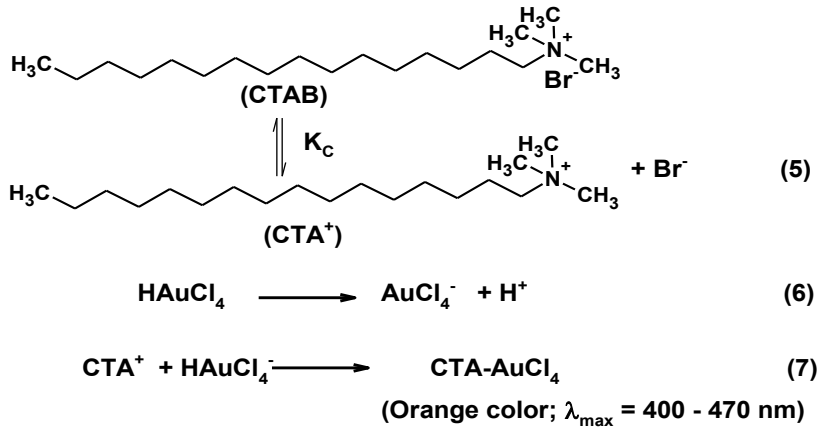
The CTAB aqueous solution is colorless. The addition of $HAuCl_4$ (pale yellow and λ_{max} = 296 nm due to the ligand to metal charge transfer) promotes the sensitive and selective complex formation with the CTAB, which decreases the distance between CTAB aggregates and $AuCl_4$ and results in the shift of the absorption peak of $HAuCl_4$ to the longer wavelength. This allows for the bare-eye detection based on color modulation of the original pale-yellow solution to orange-red, which exhibits three absorption bands at λ_{max} = 303, 409, and 464 nm. The color modulation of the pale-yellow gold solution to the orange-colored solution with CTAB confirmed the formation of CTA-$AuCl_4$ nanoaggregates, indicating the complex formation between the Au(III) and ionized CTAB. Optical images of the color changes were recorded and summarized in Scheme 1, suggesting that the intensity and color depend on the concentrations of CTAB.

The size and shape were also determined from the several TEM images (Fig. 3). It was observed that the CTA-$AuCl_4$ has a beautiful flower and/or branched- like morphology (dendrimer shape), which might be formed due to the multidirectional interaction of gold salt with the positive head groups of the CTAB aggregates. Xiao and Qi discussed the role of metal-surfactant complex-template strategy for the shape-controlled synthesis of gold nanoparticles in his pioneering review [36]. Qi et al. reported the formation of gold nanobelts by the reduction of metal-surfactant complex ($HAuCl_4$-bolaform surfactant containing two quaternary ammonium head groups) with $NaBH_4$ [37].

Ionic surfactants act as an electrolyte in aqueous solution and ionized into the corresponding anions and cations, which formed various aggregates (monomer, dimmer, trimer, etc.) at lower concentration. The micelles are formed at the critical micellar concentration (CMC), which was calculated to be 8.0×10^{-4} mol/L [43]. Surfactant monomers rapidly join and leave micelles and aggregation number represents only an average over time. Fig. 2A shows that the higher CTAB concentration has negligible effect on the absorbance of resulting orange color. Thus, we may state confidently that the aggregates of CTAB (monomer and/or dimer) interacts with the gold(III) chloride electrostatically (Scheme 2).



Scheme 1. Optical images showing the formation of different colors between the interactions of CTAB and $HAuCl_4$ at different time intervals ([CTAB] = 0.4, 1.0, and 3.0 mM, respectively, for A, B, and C).



Scheme 2. Mechanism to the formation of orange color after the addition of $HAuCl_4$ in the CTAB aqueous solution.

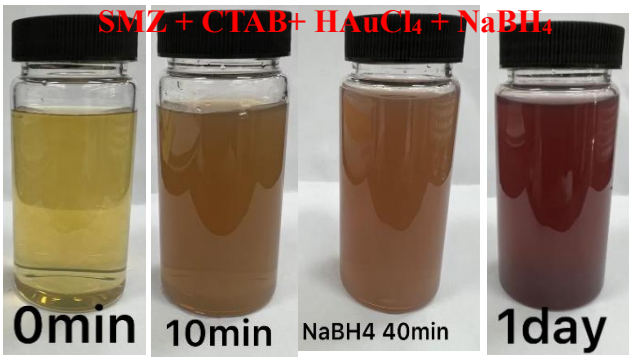
3.2. Gold nanoparticles

Fig. 4 presents UV-visible spectra of SMZ, and $HAuCl_4$, which exhibits absorption peaks at 264 nm and 296 nm, respectively, in the ultraviolet region. With the addition of the CTAB, there is a distinct and immediate bathochromic shift in λ_{max} to around 303 nm, 403 nm, and 464 nm, extending beyond this wavelength. The pale-yellow color changes to orange color immediately and the peaks intensity increases with the reaction time, probably the SMZ and $HAuCl_4$ reacts very fast with the CTAB aggregates. Interestingly, the resulting orange color also exhibits high residual absorbance from 500 to 575 nm (SPR band region of gold NPs [26, 28]), which can be attributed to the formation of CTA-$HAuCl_4$/SMZ nanoconjugates. In order to determine the morphology of as-prepared nanoconjugates, SEM and TEM images are recorded. SEM images revealed that the nanoconjugates had spherical, aggregated and layered surface morphology (Fig. 5), whereas, TEM image shows the formation of triangular nanoplate (size = 127.26 nm) of gold along with some spherical nanoparticles. TEM images also show the deposition of spherical shape NPs (size = 42.6 nm) on to the triangular nanoplate (Fig. 5).

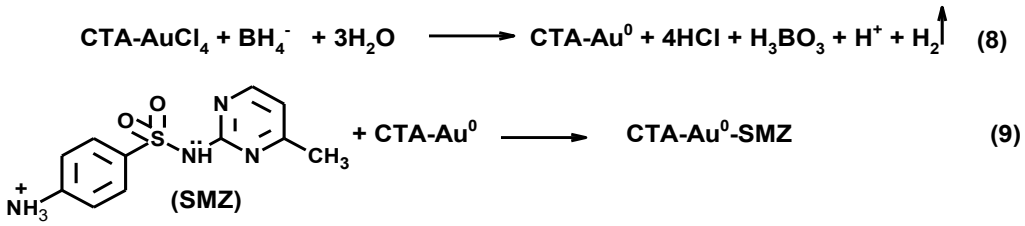
To see insight into the reduction of $HAuCl_4$ (Au(III)) to metallic gold (Au^0), UV-visible spectra of the reaction mixture (SMZ = 0.16 mM, $HAuCl_4$ = 0.4 mM, and $NaBH_4$ = 0.6 mM) were recorded in the absence (Fig. 6A) and presence of the CTAB (0.4 mM; Fig. 6B) at definite time intervals. UV-visible spectrum was featureless in the entire visible (Fig. 6A; red line). The two broad shoulders began to develop centered at 420 nm and 554 nm; as the reaction time increases, a clear and bathochromic shift is observed, diagnostic of reduction (Au(III) $\rightarrow$ Au^0) in the absence of the CTAB. Fig. 6B shows that there is clearly a progressive suppression of the orange color development in the presence of $NaBH_4$ at 403 nm. In contrast, addition of $HAuCl_4$ in the CTAB solution, as demonstrated in Figs. 1, 4, S1, and S2. This is the direct evidence that the CTA^+ binds

with the $AuCl_4^-$ via electrostatic interactions very fast, and leads to the formation of CTA-$AuCl_4$ nanoconjugates

On the other hand, absorption peaks at 403 nm and 537 nm, respectively, decrease and increase with the reaction time, respectively, in the presence of the CTAB (Fig. 6B). Finally, the UV-visible spectrum of as-prepared gold sols exhibits a sharp SPR band at 537 nm after 24h (Fig. 6B; brown), which is a characteristic of the spherical gold NPs. From the foregoing analysis, the decrease in the absorbance at 403 nm is attributed to the reduction of the CTA-$AuCl_4$ complex, whereas the increase in the absorbance at 537 nm might be due to the formation of spherical- shaped gold NPs [44]. The formation and decomposition of CTA-$AuCl_4$ can be visualized by using the required concentration of $NaBH_4$ (Fig. 6B). These results can be rationalized due to the strong reducing nature of the $NaBH_4$. Optical images were also captured of the reaction mixture containing CTAB, SMZ, $HAuCl_4$, and $NaBH_4$ at different time intervals (Scheme 3). These findings are summarized and represented in Scheme 4.



Scheme 3. Optical images of AuNPs formation by the reduction of $HAuCl_4$ with $NaBH_4$ in the presence of SMZ and CTAB.



Scheme 4. Mechanism to the formation of CTA-Au^0 (dark brown color; λ_{max} = 537 nm) and their modification with SMZ.

The morphology of AuNPs was evaluated with SEM and the images are presented in the Fig. 7. Concerning morphology, micrographs exhibit aggregates of spherical particles in the range of 27 to 59 nm. TEM images of the AuNPs are shown in Fig. 7, which depicted the occurrence of aggregated, triangular, irregular, and spherical, with sizes ranging from 17.30 nm to 31.38 nm. It was observed that the average particles had a spherical shape with size of 23.79 ± 2.7 nm (SD). The EDX spectrum analysis confirmed that the prepared NPs contained gold, carbon, and oxygen peaks, without any impurities (Fig. 8). The elemental mapping from the C-Ka edge (red), O-Ka edge (red), and Au-Ma edge (blue), shown in Fig. 8, confirm that Au is uniformly distributed on the sample surface. The presence of a band at 2.1 keV in the EDX spectrum (Fig. 8) is confirmation of the composition of > 99.9% of gold metal atoms [45].

In the XRD spectrum (Fig. 9) five prominent peaks located at 2θ values, 38.22^0, 44.37^0, 64.60^0, 77.11^0, and 81.78^0, were observed, which are characteristic of metallic gold and ascribed with hkl (111), (200), (220), (311), and (222), respectively, (JCPDS: 90-08463) [46], Bragg reflection of a face centered cubic (fcc) Au metallic structure with lattice parameters $\alpha = \beta = \gamma = 90.00^0$, and a = b = c = 4.076 Å. The XRD data of a-prepared AuNPs are summarized in Tables 1 and 2. The percent composition of metallic gold (Fig. 9) and volume of the crystal were obtained to be 100%

and 67.754 $Å^3$ from the XRD analysis, respectively. The absence of impurities implies that pure metallic gold (Au^0) was produced using the applied metal-surfactant template method.

3.3. ^1H and ^{13}C NMR data

Solution state ^1H NMR and ^{13}C NMR were recorded in order to confirm the coordination of CTAB with AuNPs. The NMR spectrum of CTA-AuNPs/SMZ was analyzed by a comparison to NMR spectrum of pure CTAB. The ^1H NMR spectrum of as-prepared AuNPs is given in Fig.10. Kavas et al. reported the five resonance peaks at 0.85 ppm (for terminal CH_3), 1.24 ppm (for bulk CH_2), 1.71 ppm (for β- CH_2), 3.10 ppm (for head group CH_3), and 3.30 ppm (for α-CH_2) of the pure CTAB [47]. For CTA-AuNPs, the resonance peaks are appeared at 0.87-0.84 ppm (triplet), 1.24 ppm, 1.66 ppm, 3.01 ppm, and 3.20-3.23 ppm (triplet), respectively, which assigned to the terminal methyl group, bulk methylene groups, β- CH_2, head group (-$N^+(CH_3)_3$), and α-CH_2 (Table ST1, supporting information). The chemical shift changes for the head group methyl protons indicates that the interaction between CTAB and metallic gold is mainly located around the head group [48]. The downfield chemical shifts were also observed for the signals of α-CH_2 and β-CH_2 protons, which can be ascribed to another interaction between CTAB and AuNPs [49]. Thus, it was concluded that the CTAB molecules associated with the AuNPs though their positive head groups.

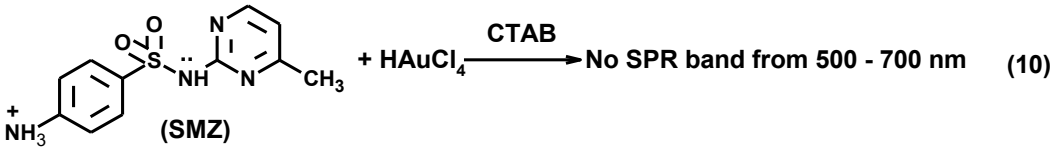
The ^{13}C NMR spectrum of as-prepared CTA-AuNPs/SMZ in DMSO is presented in Fig. 11. The resonance signals located at 14.42 ppm, 22.39-22.49 ppm, 26.1 ppm, 29.50-28.19 ppm, 32.74 ppm, 52.61 ppm, and 65.80 ppm, were observed, which are characteristic of CTA^+ and assigned to the terminal CH_3, C2, C15, C3, C4-13, C14, C-head group (-$N(CH_3)_3$, and C1, respectively. Table ST2 shows the chemical shift of the CTAB and CTA-AuNPs in solution and labelled according to the structural formula of the CTAB (Fig. 11). Therefore, CTAB molecules are present and directed the speciation of the AuNPs. These observations are in good agreement to the results of Xu et al. [49]

and Wang et al. [50] regarding the chemical shifts in the ^{13}C NMR resonance signals of CTAB in the formation of microporous molecular sieves with ZMS-5 and mesophase silicates, respectively.

The ^{1}H NMR spectra of SMZ, SMZ-$HAuCl_4$ and CTA-AuNPs/SMZ were recorded to establish the coordination of SMZ. These results are depicted in Figs. 12 and 13, while the corresponding assignments and chemical shifts are given in Table ST3. For SMZ-$HAuCl_4$, the resonance signal at 10.37 ppm (singlet) is assigned to the hydrogen of the sulfonamide group (O_2S-N-H) (Fig. 12). The appearance of a signal at 10.37 ppm indicates that SMZ is not coordinated with the gold salt precursor (SMZ + $HAuCl_4$→ no complex formation between SMZ and $HAuCl_4$). The resonance signals at 7.62-7.62 ppm, 6.57-6.56 ppm, 8.30 ppm, 6.88 ppm, and 5.98 ppm are assigned to the hydrogens of C-2/C-6, C-3/C-5, C-10, C-11, and amino group at C-1, respectively (Fig. 12). The signal appear at 2.35 ppm might be due to the methyl protons of pyrimidine ring at C-9 (Fig. 13). The signal at 2.53 ppm is assigned to the methyl group of the DMSO. The proton signal at 10.37 ppm of the sulfonamide group was not appeared in the ^{1}H NMR spectrum of CTA-AuNPs with SMZ, (Fig. 13). The above results showed that the addition of SMZ changes the ^{1}H NMR spectrum of the CTA-AuNPs. Thus, the CTA-AuNPs positive charges could be modified on to the surfaces by the SMZ to form the CTA-AuNPs/SMZ since SMZ hold amino group with negative charges in acidic solution due to the ionization of sulphonic group hydrogen (-O_2S-NH- → -O_2S-N^-- + H^+).

The carbon NMR spectrum of CTA-AuNPs/SMZ is presented in Fig. 14, while their chemical shifts are given in Table ST3 along with the resonance signals of pure SMZ. For CTA-AuNPs/SMZ, The carbon atoms of the pyrimidine ring are most shifted. Thus, confirming the coordination of SMZ on to the positive surface of CTA-AuNPs via electrostatic interaction as well as van der Waals forces [35, 36, 48]. The morphology of as-prepared AuNPs could be adjusted by changing the mixing ratio between cationic surfactant (CTAB) and $HAuCl_4$ in the reaction

solution. On the basis of above results, we may conclude that the no SPR band appeared from 500 to 700 nm (characteristic range of the gold NPs) in the reaction mixture containing $HAuCl_4$, CTAB, and SMZ at room temperature (Eq. (10). The SPR band at 537 nm was appeared after the addition of $NaBH_4$, (Fig. 6B) which indicates the formation of CTA-AuNPs/SMZ.



4. Conclusion

In summary, we have successfully prepared CTA-$AuCl_4$ orange colored nanoconjugates using CTAB and $HAuCl_4$. The role of CTAB surfactant was carefully studied. The characterization of the existence, status, and content of CTAB in CTA-$AuCl_4$ was performed by UV-visible and TEM analysis. CTA-$AuCl_4$ was used for the synthesis of AuNPs. SMZ is not in a position to reduce coordinated gold salt into the metallic gold (Au^0) with and without CTAB. The $NaBH_4$ was added into the reaction mixture as a reductant, and brown-purple-colored gold sols were formed, having a sharp well-defined SPR band of metallic gold at 537 nm. The existence of CTAB and SMZ in the as-prepared AuNPs was confirmed by the ^1H NMR, ^{13}C NMR, FTIR, UV-visible, and XRD analysis. The results indicate that CTAB acts as a structure-directing agent without any decomposition, and the hydrophilic head group coordinates with the $HAuCl_4$. To the best of our knowledge, this is the first time that CTA-$AuCl_4$ has been used as a metal-surfactant complex template for the synthesis of AuNPs. This finding may provide a new insight into the molecular factors governing the formation of CTA-$AuCl_4$ and their simultaneous reduction to the AuNPs for practical applications.

Acknowledgement

The authors gratefully acknowledge the Deanship of Scientific Research (DSR) at King Abdulaziz University, Jeddah, Saudi Arabia, for funding this project under grant No. (IPP: 452-247-2026) and for providing technical support.

CRediT authorship contribution statement

Zoya Zaheer: Writing – review & editing, Writing – original draft, Supervision, Methodology, Conceptualization. **Huda Razayq Alyoubi:** Data curation, Investigation, Writing – review & editing. **Wafa A. Bawazir**: Data curation, Writing – review & editing, Writing – original draft, Supervision, Methodology, Conceptualization.

Declaration of competing interest

The authors declare that they have no known competing financial interests or personal relationships that could have appeared to influence the work reported in this paper.

Data availability

Data will be made available on request.

References

[1] T. Sakai, A. Hirose, Mixed ternary ion associate formation between xanthene dye, cinchona-alkaloid and quaternary ammonium ion and its application to the determination of trace amounts of quaternary ammonium salts in pharmaceuticals, Talanta 59 (2003)167-175.

[2] V. Kubicek, K. Nemcova, Study of the interaction phenomena of cetyl-trimethyl ammonium bromide, cetylpyridinium chloride and benzethonium chloride with C. I. Acid Orange 52 and picric acid by two spectral methods, Dyes Pigm. 68 (2006) 183-189.

[3] R. T. Buwalda, J. B. F. N. Engberts, Aggregation of dicationic surfactants with methyl orange in aqueous solution, Langmuir 17 (2001) 1054-1059.

[4] M. Dakiky, A. Manassra, M. Abdul Kareem, F. Jumean, M. Khamis, Acid Alizarin Violet Interactions with Surfactants: Ionization and Thermodynamic Parameters in Buffered Cationic, Anionic and Nonionic Surfactant Solutions, Dyes Pigm. 63 (2004) 101-113.

[5] L. K. Wang, D. F. Langley, Determining cationic surfactant concentration, Ind. Eng. Chem. Prod. Res. Dev. 14 (1975) 210-212.

[6] Y. Chang, N. Dou, M. Liu, M. Jiang, J. Men, Y. Cui, R. Li, Y. Zhu, Efficient removal of anionic dyes from aqueous solution using CTAB and β-cyclodextrin-induced dye aggregation, J. Mol. Liq. 309 (2020) 113021.

[7] L. Zhu, J. Ma, Simultaneous removal of acid dye and cationic surfactant from water by bentonite in one-step process, Chem. Eng. J. 139 (2008) 503-509.

[8] M. S. Bakshi, How surfactants control crystal growth of nanomaterials, Cryst. Growth Des. 16 (2016) 1104-1133.

[9] M. S. Bakshi, A simple method of superlattice formation: step-by-step evaluation of crystal growth of gold nanoparticles through seed- growth method, Langmuir 25 (2009) 12697-12705.

[10] T. K. Sau, C. J. Murphy, Self-Assembly Patterns Formed upon Solvent Evaporation of Aqueous Cetyltrimethylammonium Bromide-Coated Gold Nanoparticles of Various Shapes, Langmuir 21 (2005) 2923-2929.

[11] Z. Zaheer, H. Alsubaie, S. A. Kosa, E. S. Aazam, Insights into the role of ionic surfactants on the morphology of gold and gold@ silver nanoparticles, J. Mol. Liq. 400 (2024) 124565.

[12] Z. Zaheer, Silver nanoparticles to self-assembled films: green synthesis and characterization, Colloids surf. B: Biointerfaces 90 (2012) 48-52.

[13] S. A. Al-thabaiti, A. Y. Obaid, Z. Khan, O. Bashir, S. Hussain, Cu nanoparticles: synthesis, crystallographic characterization, and stability, Colloid Polym. Sci. 293 (2015), 2543-2554.

[14] E.C. Dreaden, A.M. Alkilany, X. Huang, C.J. Murphy, M.A. El-Sayed, The golden age: gold nanoparticles for biomedicine, Chem. Soc. Rev. 41 (2012) 2740-2779.

[15] J. Pérez-Juste, I. Pastoriza-Santos, L. Liz-Marzán, P. Mulvaney, Gold nanorods: synthesis, characterization and applications, Coord. Chem. Rev. 249 (2005) 1870-1901.

[16] B. Nikoobakht, M.A. El-Sayed, Evidence for bilayer assembly of cationic surfactants on the surface of gold nanorods, Langmuir 17 (2001) 6368-6374.

[17] Z. Khan, T. Singh, J. I. Hussain, A. A. Hashmi, Au(III)-CTAB reduction by ascorbic acid: Preparation and characterization of gold nanoparticles, Colloids Surf. B: Biointerfaces, 104 (2013)11-17.

[18] Z. Khan, S. A. Al-Thabaiti, O. Bashir, Natural sugar surfactant capped gold nano-disks: Aggregation, green synthesis and morphology, Dyes Pigm. 124 (2016) 210-221.

[19] E. S. Aazam, Z. Zaheer, Gold@Silver bimetallic: Fabrication and removal of toxic chromium (VI), J. Mater. Sci.: Mater. Electron. 32 (2021) 11043-11058.

[20] E. S. Aazam, Z. Zaheer, Rose cyanidin 3,5-di-O-glucoside assisted gold nanoparticles, their antiradical, and photocatalytic activities, J. Mater. Sci.: Mater. Electronics, 31 (2020) 8780-8795.

[21] M. Compagnoni, S. A. Kondrat, C. E. Chan-Thaw, D. J. Morgan, D. Wang, L. Prati, A. Villa, N. Dimitratos, I. Rossetti, Spectroscopic investigation of Titania-supported gold nanoparticles prepared by a modified deposition/precipitation method for the oxidation of CO, ChemCatChem. 8 (2016, 2136-2145.

[22] Y. Zhao, Y. Huang, H. Zhu, Q. Zhu, Y. Xia, Three-in-one: sensing, self-assembly, and cascade catalysis of cyclodextrin modified gold nanoparticles, J. Am. Chem. Soc. 138 (2016) 16645-16654.

[23] P. Singh, S. Roy, A. Jaiswal, Cubic gold nanorattles with a solid octahedral core and porous shell as efficient catalyst: immobilization and kinetic analysis, J. Phys. Chem. C 121 (2017) 22914-22925.

[24] J. Zheng, X. Cheng, H. Zhang, X. Bai, R. Ai, L. Shao, J. Wang, Gold nanorods: the most versatile plasmonic nanoparticles, Chem. Rev. 121 (2021) 13342-13453.

[25] A. Ma, W. Yang, H. Yan, J. Tang, Substrate-free fabrication of single-crystal two-dimensional gold nanoplates for catalytic application, Langmuir 38 (2022) 15263-15271.

[26] M. Gul, M. Kashif, S. Muhammad, S. Azizi, H. Sun, Various methods of synthesis and applications of gold-based nanomaterials: A detailed review, Cryst. Growth Des. 25 (2025) 2227-2266.

[27] M.R. Langille, M.L. Personick, J. Zhang, C.A. Mirkin, Defining rules for the shape evolution of gold nanoparticles, J. Am. Chem. Soc. 134 (2012) 14542-14554.

[28] T. Dinh, Z. Dobo, A. B. Palotas, H. Kovacs, A review of gold nanoparticle synthesis: Transitioning from conventional techniques to plant-mediated green nanofabrication, Mater. Today Chem. 48 (2025) 103003.

[29] J. He, S. Unser, I. Bruzas, R. Cary, Z. Shi, R. Mehra, K. Aron, L. Sagle, The facile removal of CTAB from the surface of gold nanorods, Colloids Surf. B: Biointerfaces 163 (2018) 140-145.

[30] X.-Y. Liu, Z.-L. Zhao, T.-T. Hao, X. Li, A simply visual and rapidly colorimetric detection of Hg^{2+} in cosmetics based on gold nanoparticles modified by sulfadiazine, Optical Mater.137 (2023)113622.

[31] Z. Niu, Y. Liu, X. Li, H. Zhu, M. Zhang, K. Yan, H. Chen, Colorimetric detection of sulfamethazine based on target resolved calixarene derivative stabilized gold nanoparticles aggregation, Microchimica Acta, 189 (2022) p1.

[32] J. Shah, R. Purohit, R. Singh, A. S. Karakoti, S. Singh, J. Colloid Interface Sci. 456 (2015)100-107.

[33] M. Yang, X. Wu, X. Hu, K. Wang, C. Zhang, E. Gyimah, S. Yakubu, Z. Zhang, Electrochemical immunosensor based on Ag^{+}-dependent CTAB-AuNPs for ultrasensitive detection of sulfamethazine, Biosens. Bioelectron. 144 (2019) 111643.

[34] J. Zhang, W. Zheng, X. Jiang, Ag^{+}-gated surface chemistry of gold nanoparticles and colorimetric detection of acetylcholinesterase, Small 14 (2018) e1801680.

[35] J. Xiao, L. Qi, Surfactant-assisted, shape-controlled synthesis of gold nanocrystals, Nanoscale, 3 (2011) 1383-1396.

[36] L. Li, Z. Wang, T. Huang, J. Xie, L. Qi, Porous gold nanobelts templated by metal-surfactant complex nanobelts, Langmuir, 26 (2010)12330-12335.

[37] R. Kaur, S. K. Mehta, Self aggregating metal surfactant complexes: Precursors for nanostructures, Coord. Chem. Rev. 262 (2014) 37-54.

[38] C. J. Jia, F. Schuth, Colloidal metal nanoparticles as a component of designed catalyst, Phys. Chem. Chem. Phys. 13 (2011) 2457-2487.

[39] H. R. Alyoubi, E. A. Saleh, W. A. Bawazir, Z. Zaheer, Sulfamerazine-functionalized silver nanoparticles with cetyltrimethylammonium bromide and their interactions with eosin yellow, J. Mol. Struct. 1367 (2026) 146123.

[40] X. Lu, M. S. Yavuz, H.-Y. Tuan, B. A. Korgel, Y. Xia, Ultrathin gold nanowires can be obtained by reducing polymeric strands of oleylamine-AuCl complexes formed via aurophilic interaction, J. Am. Chem. Soc. 130 (2008) 8900-8901.

[41] P.H. Connett, W.H. Wetterhahn, In vitro reaction of the carcinogen chromate with cellular thiols and carboxylic acids, J. Am. Chem. Soc. 107 (1985) 4282-4288.

[42] M. A. Malik, S. A. AL-Thabaiti, Z. Khan, Kinetics of oxidation of d-glucose by permanganate in aqueous solution of cetyltrimethylammonium bromide, Colloids Surf. A: Physicochem. Eng. Aspects 337 (2009) 9-14.

[43] Z. Zaheer, Rafiuddin, Sub- and post-micellar catalytic and inhibitory effects of cetyltrimethylammonium bromide in the permanganate oxidation of phenylalanine, Colloids Surf. B: Biointerfaces 69 (2009) 251-256.

[44] Z. Zhong, S. Patskovskyy, P. Bouvrette, J. H. T. Luong, A. Gedanken, The surface chemistry of Au colloids and their interactions with functional amino acids, J. Phys. Chem. B 108 (2004) 4046-4052.

[45] H. Yuan, W. Ma, C. Chen, J. Zhao, J. Liu, H. Zhu, X. Gao, Shape and SPR evolution of thorny gold nanoparticles promoted by silver ions, Chem. Mater. 19 (2007) 1592-1600.

[46] C. Feng, L. Gu, D. Yang, J. Hu, G. Lu, X. Huang, Size-controllable gold nanoparticles stabilized by PDEAEMA-based double hydrophilic graft copolymer, Polymer 50 (2009) 3990-3996.

[47] H. Kavas, Z. Durmus, M.Senel, S. Kazan, A. Baykal, M. S. Toprak, CTAB-Mn_3O_4 nanocomposites: Synthesis, NMR and low temperature EPR studies, Polyhedron 29 (2010) 1375-1380.

[48] A. M. Al-Balawi, Z. Zaheer, S. A. Kosa, Facile synthesis of silver-rhenium with plasmonic and mesoporous properties, J. Mol. Struct. 1291 (2023) 135978.

[49] D. Xu, J. Feng. S. Che, An insight into the role of the surfactant CTAB in the formation of microporous molecular sieves, Dalton Trans. 43 (2014) 3612-3617.

[50] L.Q. Wang, J. Liu, G.J. Exarhos, B.C. Bunker, Investigation of the structure and dynamics of surfactant molecules in mesophase silicates using solid-state^{13} C NMR, Langmuir 12 (1996) 2663-2669.

Table 1. Space group, structural parameter, and lattice constant of CTA-AuNPs/SMZ.

Qualitative analysis							
Phase name	Formula	Space group					DB card number
Gold	Au	225: $Fm\bar{3}m$					9008463
Structure parameter							
Phase	Element	x	y	z		Occupancy	Temperature factor
Gold	Au	0.0000	0.0000	0.0000		1.000	0.500
Lattice constant	a (Å)	b (Å)	c (Å)	α (^{0})	β (^{0})	γ (^{0})	V (Å^3)
Gold	4.076	4.076	4.076	90.00	90.00	90.00	67.754

Table 2. XRD peaks position, Millar indices, crystallite diameter, and interplanar spacing of the CTA-AuNPs/SMZ.

2θ of the intense peaks (^{0})	FWMH β (^{0})	Millar indices (hkl)	Crystallite diameter, D (nm)	Interplanar spacing, d (nm)
38.22	0.51	111	6.564	0.247
44.37	0.73	200	5.432	0.203
64.60	0.56	220	4.091	0.145
77.66	0.43	311	3.450	0.132
81.78	0.25	222	2.018	0.125
Average values (nm)			4.311± 3.5(Mean ± SD)	0.155

Figure captions:

Fig. 1. UV-visible spectra of $HAuCl_4$ with CTAB as a function of time (Experimental conditions: [$HAuCl_4$] = 0.6 mM, [CTAB] = 1.0 mM (A), and 2.0 mM (B)).

Fig. 2. Effect of CTAB on the absorbance of CTA-$AuCl_4$ ion-pair formation (A) and calculation of ion-pair formation constant (B) (Experimental conditions: [$HAuCl_4$] = 0.6 mM).

Fig. 3. TEM images of CTA-$AuCl_4$ nanoconjugates for the Fig. 1A data.

Fig. 4. UV-visible spectra of $HAuCl_4$, SMZ and CTAB as a function of time (Experimental conditions: [$HAuCl_4$] = 0.6 mM, [CTAB] = 1.0 mM, and [SDZ] = 0.10 mM.

Fig. 5. SEM and TEM images of CTA-$AuCl_4$/SMZ nanoconjugates for the Fig. 4 reaction conditions.

Fig. 6. UV-visible spectra of reaction mixture ($HAuCl_4$, SMZ, and CTAB) in the presence of $NaBH_4$ (0.6 mM) as a function of time (Experimental conditions: [$HAuCl_4$] = 0.4 mM, [SMZ] = 0.16 mM, and [CTAB] = 0.0 (A), and 0.4 mM (B).

Fig. 7. SEM and TEM images of CTA-AuNPs/SMZ for the Fig. 6B reaction conditions.

Fig.8. SEM elemental mapping and EDX of CTA-AuNPs/SMZ for the Fig. 6 reaction conditions.

Fig. 9. XRD patterns of CTA-AuNPs/SMZ for the Fig. 6 reaction conditions.

Fig. 10. ^{1}H NMR spectrum of CTAB in CTA-AuNPs/SMZ.

Fig. 11. ^{13}C NMR spectrum of CTAB in CTA-AuNPs/SMZ.

Fig. 12. ^{1}H NMR spectrum of SMZ-$HAuCl_4$.

Fig. 13. ^{1}H NMR spectrum of SMZ in CTA-AuNPs/SMZ.

Fig. 14. ^{13}C NMR spectrum of SMZ in CTA-AuNPs/SMZ.

Fig.1A

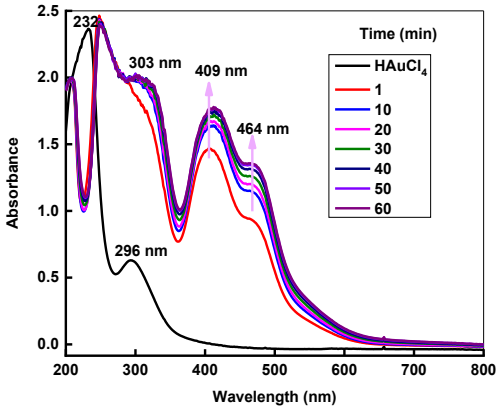

232
303 nm
409 nm
464 nm
296 nm
Time (min)
HAuCl4
1
10
20
30
40
50
60
Absorbance
Wavelength (nm)

Fig.1B

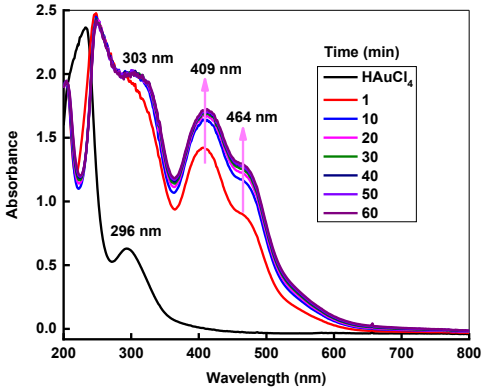

303 nm
409 nm
464 nm
296 nm
Time (min)
HAuCl4
1
10
20
30
40
50
60
Absorbance
Wavelength (nm)

Fig.2A

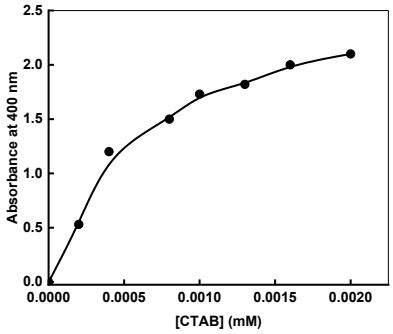

Absorbance at 400 nm
2.5
2.0
1.5
1.0
0.5
0.0
0.0000
0.0005
0.0010
0.0015
0.0020
[CTAB] (mM)

Fig.2B

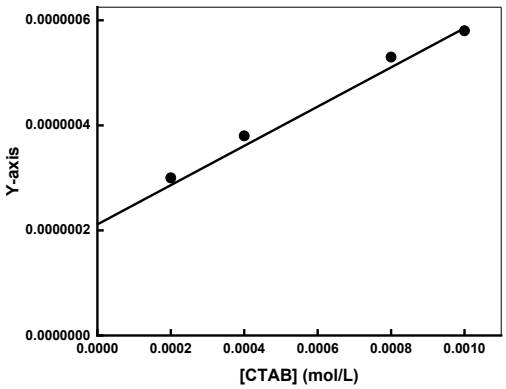

Y-axis
0.0000006
0.0000004
0.0000002
0.0000000
0.0000
0.0002
0.0004
0.0006
0.0008
0.0010
[CTAB] (mol/L)

Fig. 3.

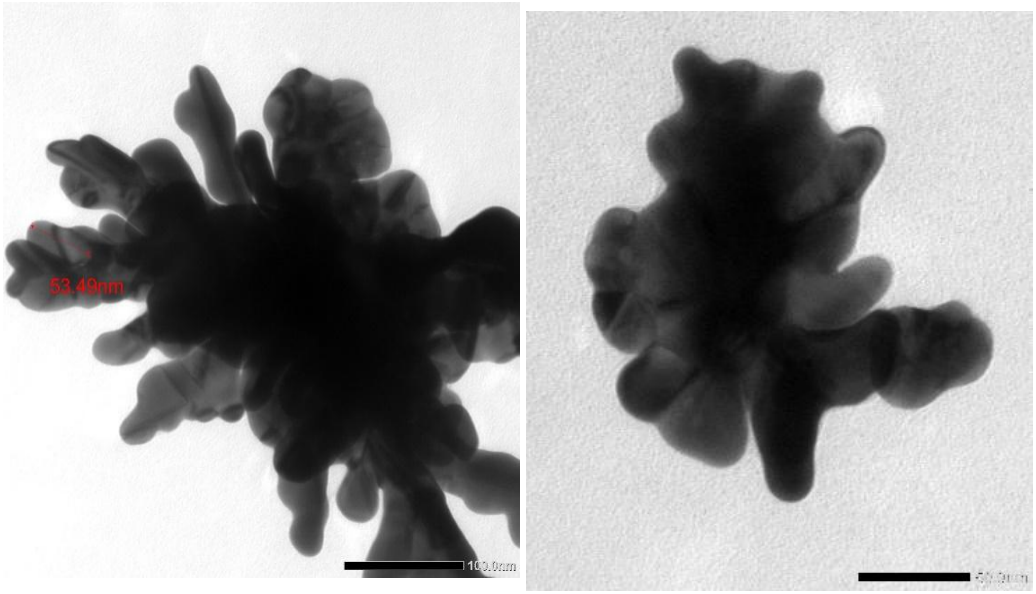


Fig. 4.

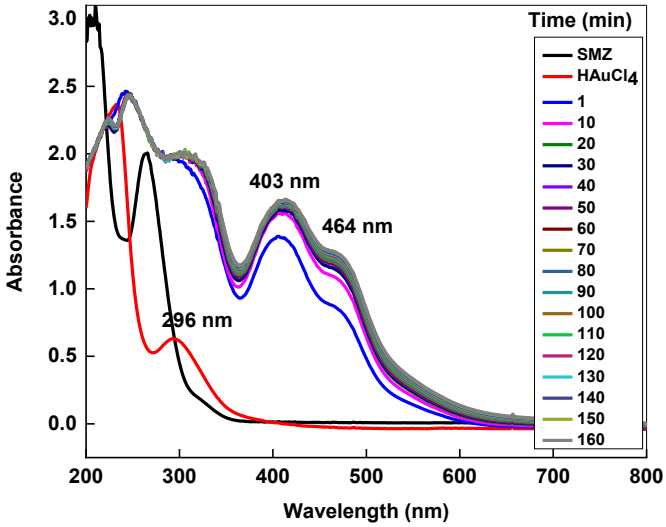

Time (min)
SMZ
HAuCl4
1
10
20
30
40
50
60
70
80
90
100
110
120
130
140
150
160
403 nm
464 nm
296 nm
Absorbance
Wavelength (nm)
3.0
2.5
2.0
1.5
1.0
0.5
0.0
200
300
400
500
600
700
800

Fig. 5.

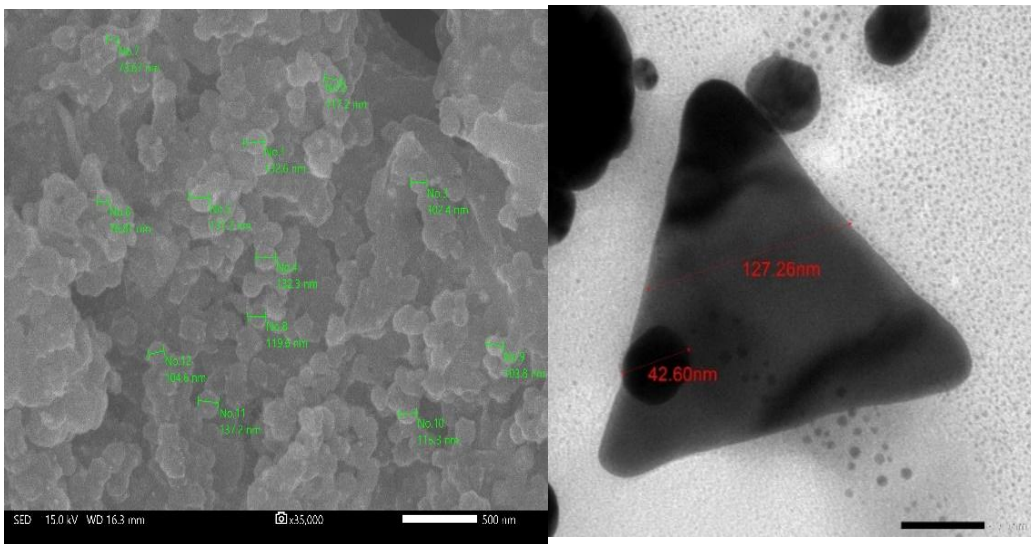


Fig. 6A

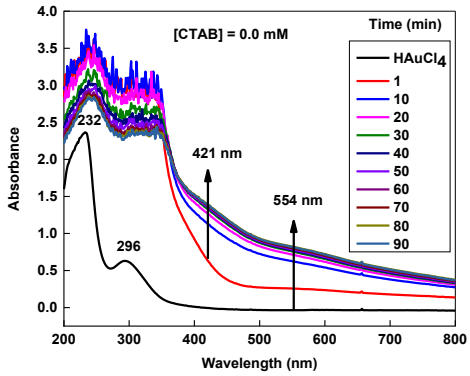

[CTAB] = 0.0 mM
Time (min)
HAuCl4
1
10
20
30
40
50
60
70
80
90
232
296
421 nm
554 nm
Absorbance
Wavelength (nm)

Fig. 6B

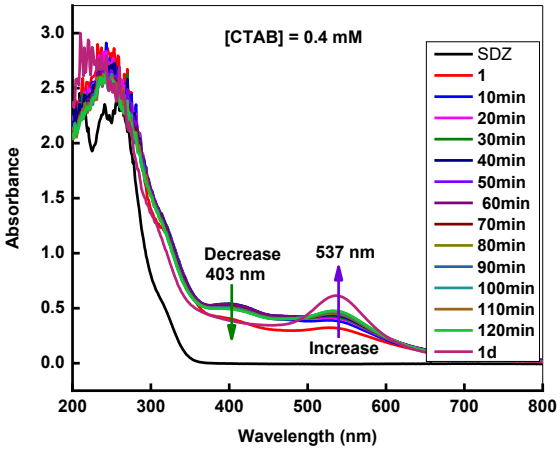

[CTAB] = 0.4 mM
SDZ
1
10min
20min
30min
40min
50min
60min
70min
80min
90min
100min
110min
120min
1d
Decrease
403 nm
537 nm
Increase
Absorbance
Wavelength (nm)

Fig. 7.

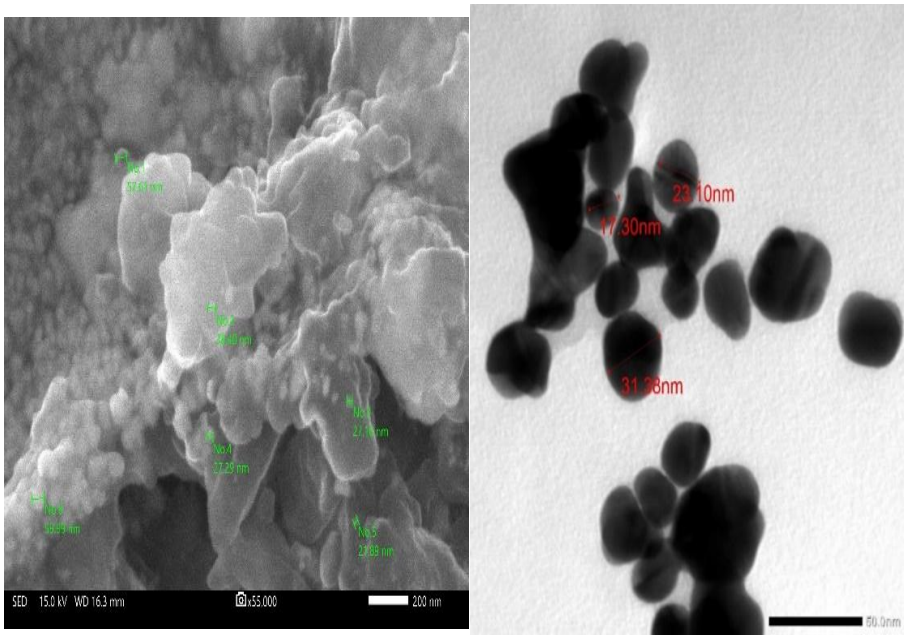
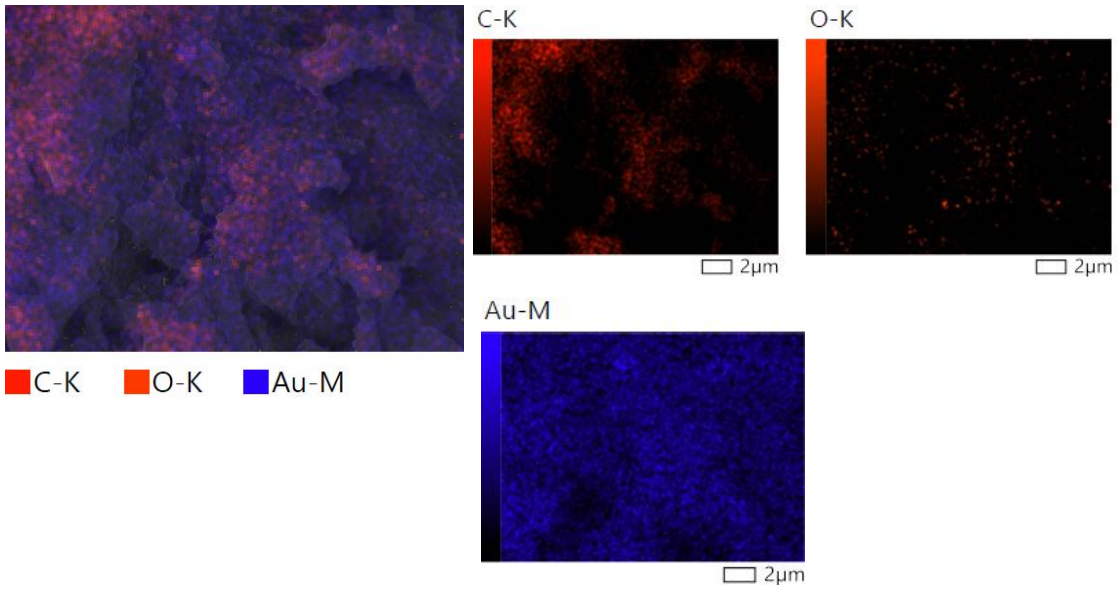


Fig. 8.


C-K
O-K
Au-M
2µm
2µm
2µm
C-K
O-K
Au-M

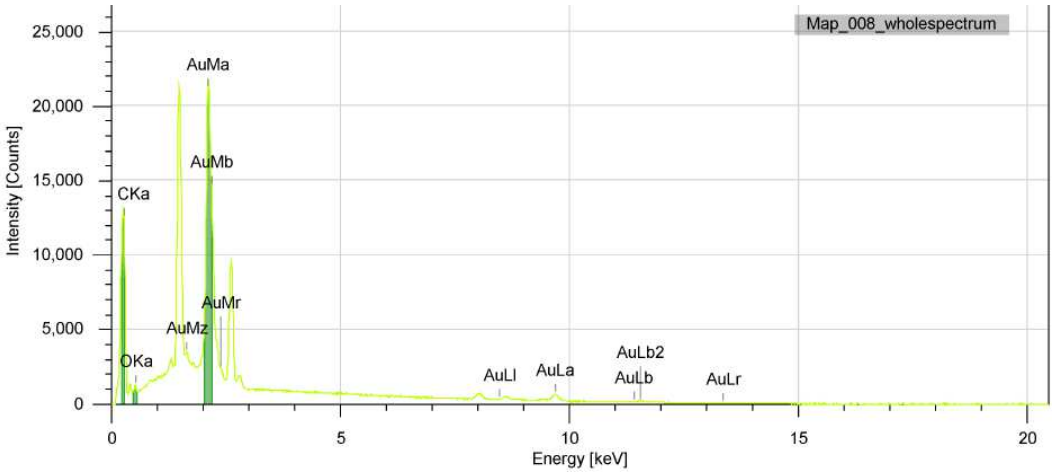

Map_008_wholespectrum
Intensity [Counts]
Energy [keV]
AuMa
AuMb
CKa
AuMr
AuMz
OKa
AuLl
AuLa
AuLb2
AuLb
AuLr
25,000
20,000
15,000
10,000
5,000
0
0
5
10
15
20

Fig. 9.

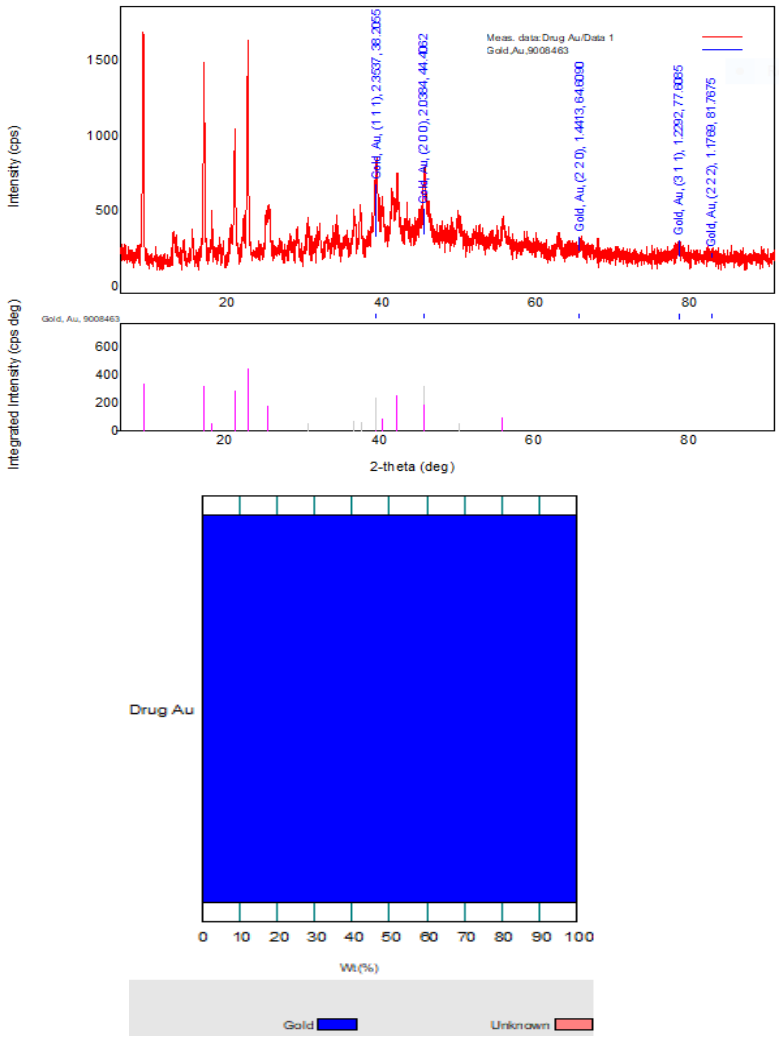

Meas. data:Drug Au/Data 1
Gold,Au,9008463
Intensity (cps)
Integrated Intensity (cps deg)
2-theta (deg)
Drug Au
Wt(%)
Gold
Unknown

Fig. 10.

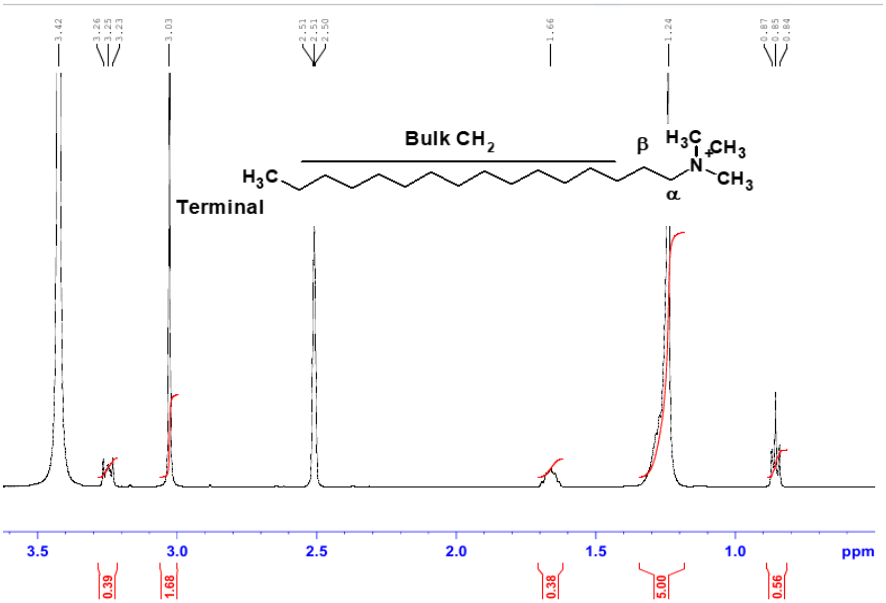

Bulk CH2
β
H3C
CH3
N+
CH3
H3C
Terminal
α
3.5
3.0
2.5
2.0
1.5
1.0
ppm
0.39
1.68
0.38
5.00
0.56

Fig. 11.

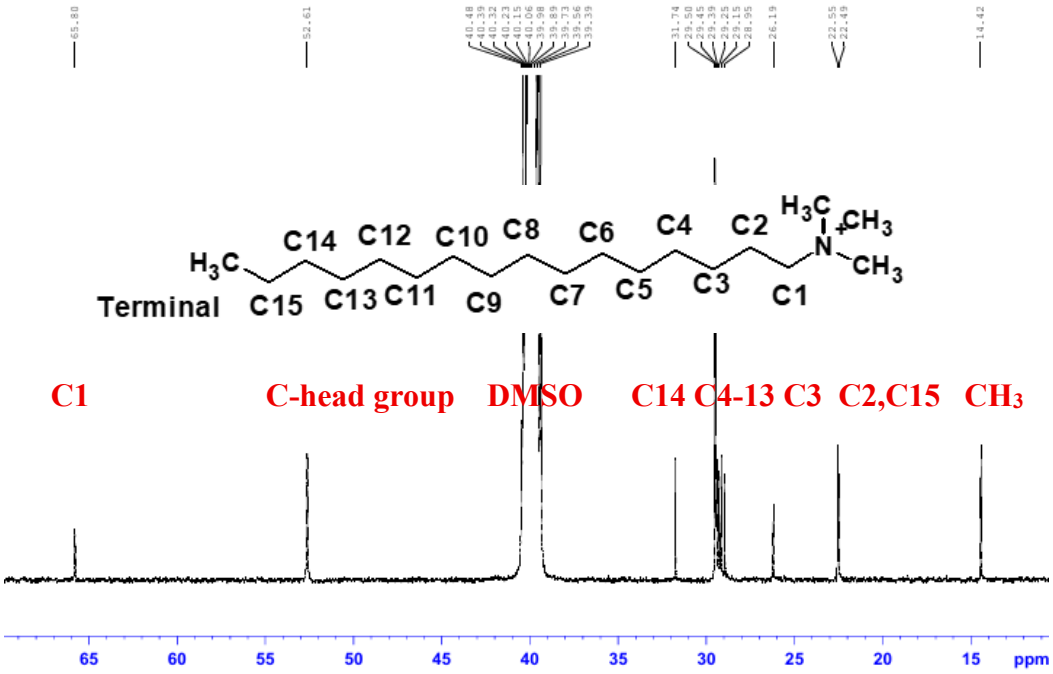

65.80
52.61
40.48
40.39
40.32
40.23
40.15
40.06
39.89
39.73
39.56
39.39
31.74
29.50
29.45
29.39
29.25
29.15
28.95
26.19
22.55
22.49
14.42
H3C
C14
C12
C10
C8
C6
C4
C2
H3C
CH3
N
CH3
Terminal
C15
C13
C11
C9
C7
C5
C3
C1
C1
C-head group
DMSO
C14
C4-13
C3
C2,C15
CH3
65
60
55
50
45
40
35
30
25
20
15
ppm

Fig. 12.

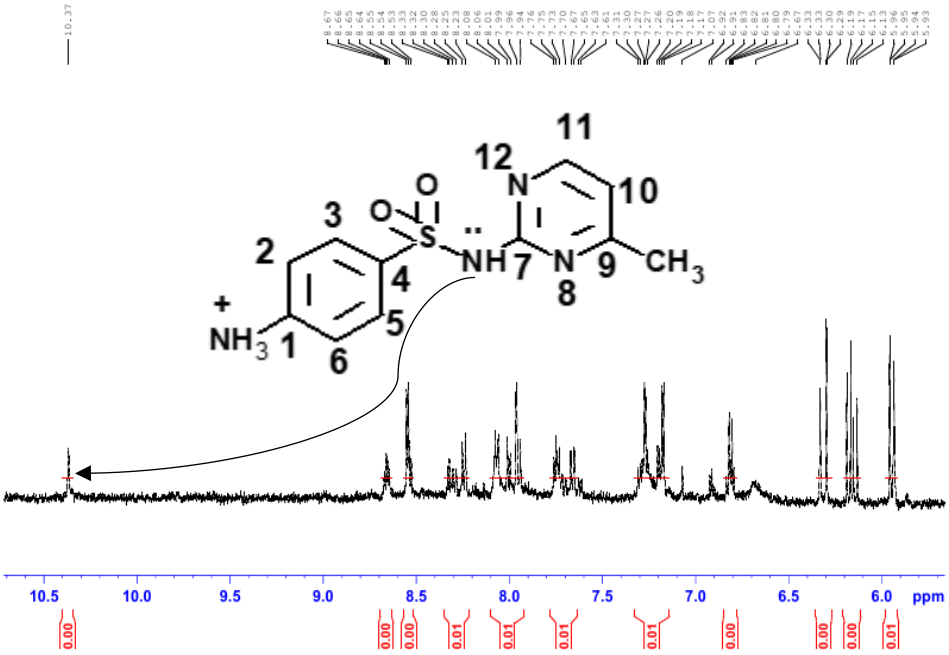

11
12
N
10
O
O
3
S
2
NH
7
N
9
CH3
4
8
+
NH3
1
5
6
10.5
10.0
9.5
9.0
8.5
8.0
7.5
7.0
6.5
6.0
ppm

Fig. 13.

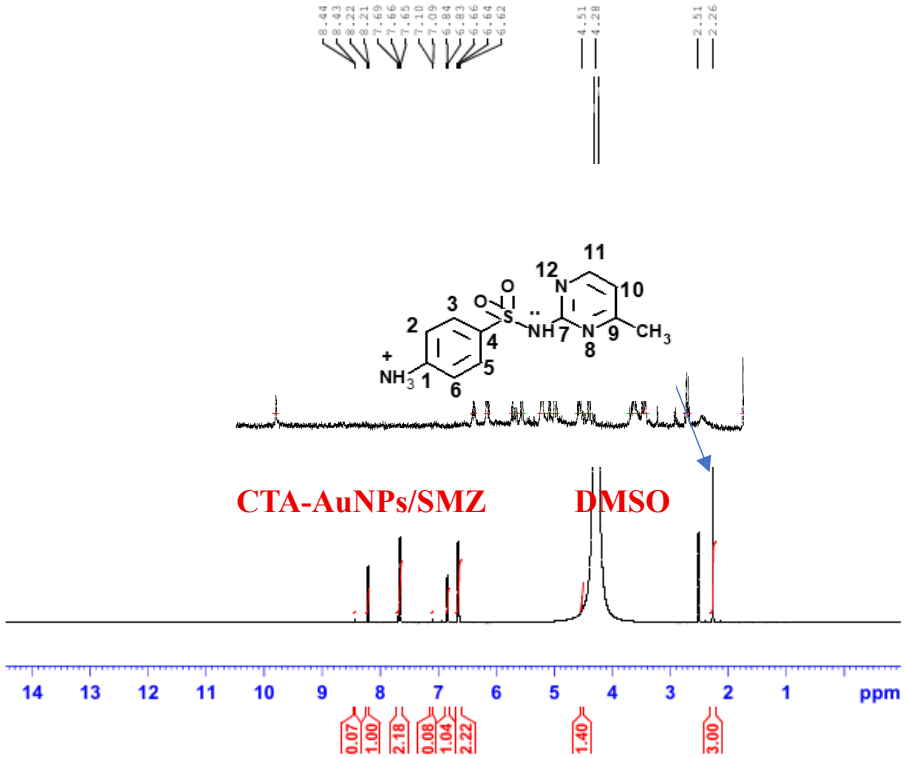
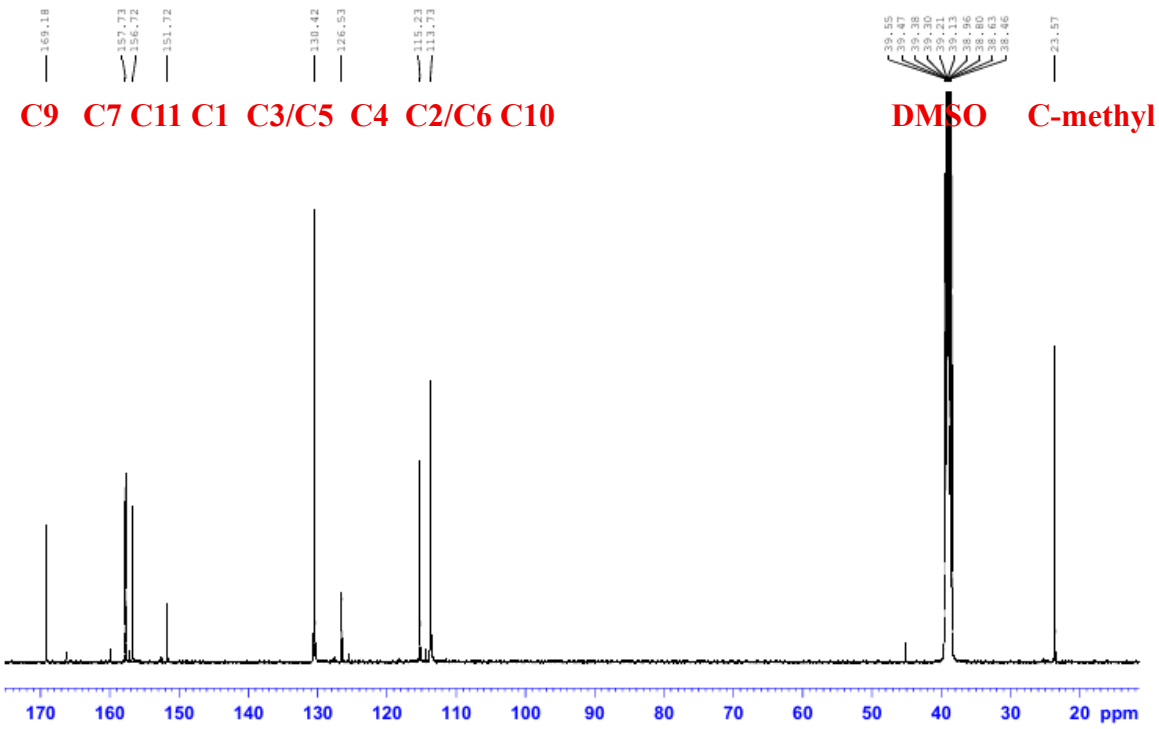

8.44
8.43
8.22
8.21
7.69
7.66
7.65
7.10
7.09
6.84
6.83
6.66
6.64
6.62
4.51
4.28
2.51
2.26
CTA-AuNPs/SMZ
DMSO
14
13
12
11
10
9
8
7
6
5
4
3
2
1
ppm
0.07
1.00
2.18
0.08
1.04
2.22
1.40
3.00

Fig. 14.


169.18
157.73
156.72
151.72
130.42
126.53
115.23
113.73
39.55
39.47
39.38
39.30
39.21
39.13
38.96
38.80
38.63
38.46
23.57
C9
C7
C11
C1
C3/C5
C4
C2/C6
C10
DMSO
C-methyl
170
160
150
140
130
120
110
100
90
80
70
60
50
40
30
20
ppm

Supplementary Files

This is a list of supplementary files associated with this preprint. Click to download.

- Supportinginformationgold.docx